

Detection of Intermittent Faults Based on an Optimally Weighted Moving Average T^2 Control Chart with Stationary Gaussian Observations

Yinghong Zhao^{a,c}, Xiao He^a, Junfeng Zhang^a, Hongquan Ji^b, Donghua Zhou^{b,a,*}, Michael G. Pecht^c

^aDepartment of Automation, Beijing National Research Center for Information Science and Technology (BNRist), Tsinghua University, Beijing 100084, China

^bCollege of Electrical Engineering and Automation, Shandong University of Science and Technology, Qingdao 266590, China

^cCenter for Advanced Life Cycle Engineering (CALCE), University of Maryland, College Park, MD 20742, USA

Abstract

The moving average (MA) technique, also known as the smoothing technique, has been well established within the multivariate statistical process monitoring (MSPM) framework since the 1990s. However, it is still limited to handling independent data, and the optimality of its equal weight scheme remains unproven. This paper aims to weaken the independence assumption in the existing MA technique, and then extend it to a broader area of dealing with autocorrelated stationary process, giving birth to a weighted moving average (WMA) technique. The WMA technique is combined with the Hotelling's T^2 statistic to form a WMA T^2 control chart (WMA-TCC), in order to detect a more challenging type of fault, i.e., intermittent fault (IF). Different from the MA technique that puts an equal weight on samples within a time window, WMA-TCC uses correlation (autocorrelation and cross-correlation) information to find an optimal weight vector for the purpose of IF detection (IFD). In order to achieve a best IFD performance, the concept of IF detectability is defined and corresponding detectability conditions are provided, which further serve as selection criteria of the optimal weight. Then, the optimal weight is given in the form of a solution to nonlinear equations, whose existence is proven with the aid of the Brouwer fixed-point theory. Moreover, symmetrical structure of the optimal weight is revealed, and the optimality of an equal weight scheme when data exhibit no autocorrelation is proven. Finally, simulations on a numerical example and the continuous stirred tank reactor process are carried out to give a comprehensive comparison among WMA-TCC and several existing static and dynamic MSPM methods. The results show a superior IFD performance of the developed methods.

Keywords: Weighted moving average, optimal weight, intermittent faults, fault detection and detectability

1. Introduction

Fault detection (FD) for industrial processes by multivariate statistical process monitoring (MSPM) methods has been a hot topic in the past few decades [1, 2].

MSPM methods use various control charts to check statistical properties of process variables, among which T^2 control chart is one of the most effective ones since the Hotelling's T^2 statistic is admissible and powerful in certain classes of hypothesis tests [3]. It is worth mentioning that existing MSPM methods in the literature mainly focus on permanent faults (PFs), i.e., assuming once faults occur, they take effect permanently unless removed by external intervention. But more importantly, several studies [4–6] have shown that, in practice, many kinds of PF evolve gradually from intermittent faults (IFs). That is to say, IF is a prelude to PF. This implies that if faults are detected in this early stage, severe damage caused by PFs, such as system disruptions, plant shutdowns and even safety accidents, can be effectively avoided. IFs have been recently of noticeable interest [7–9], and thus a review of their current research

*This work was supported by National Natural Science Foundation of China (NSFC) under Grants 61490701, 61751307, 61522309, 61473163, 61733009, 61573377, China's Ministry of Industry and Information Technology under the R&D project of intelligent ship 1.0 ([2016]544), Special Fund of Suzhou-Tsinghua Innovation Leading Action under Grant 2016SZ0202, and Research Fund for the Taishan Scholar Project of Shandong Province of China (LZB2015-162). Corresponding author: Donghua Zhou.

Email addresses: zyh14@mails.tsinghua.edu.cn (Yinghong Zhao), hexiao@mail.tsinghua.edu.cn (Xiao He), jf-zhang13@mails.tsinghua.edu.cn (Junfeng Zhang), jihongquansd@126.com (Hongquan Ji), zdh@mail.tsinghua.edu.cn (Donghua Zhou), pecht@umd.edu (Michael G. Pecht)

status has been published [10].

The IF is a kind of non-permanent fault that lasts a limited period of time and then disappears without any treatment [10]. The IF detection (IFD) and detectability problems in discrete event systems have been studied in [7, 11, 12] based on automata, and in [13] based on Petri nets. Timed failure propagation graphs (TFPGs) can model the dynamic evolution of failure propagation over time in practical systems. In [14], the TFPG model has been modified to make it detect IFs. For a class of linear stochastic systems with IFs, a set of sliding-window-based residuals has been designed and a robust detection scheme has been adopted [15, 16]. Additionally, detection of IFs has been studied for linear time-varying systems subject to stochastic parameter uncertainty and limited resolution [8]. However, prior knowledge of the system model is required for these methods. As for data-driven methods, wavelet transform, short-time fourier transform and undecimated discrete wavelet transform have been utilized to detect intermittent electrical and mechanical faults in synchronous motors [17, 18]. In addition, combining the spectral kurtosis of vibration signals with k -nearest neighbor distance analyses, a new method [19] has been developed to detect intermittent bearing faults in electric motors. Note that these signal-analysis-based methods are suitable to process unidimensional signals that possess periodicity. Moreover, the decision forest [9] and dynamic Bayesian network [20] have also been presented to detect IFs in industrial systems, whereas historical data of various faults are needed.

So far, the IFD problems have not been fully investigated in the MSPM framework, where high-dimensional and correlated variables are easy to handle and historical fault data are not necessary. Generally speaking, IFs have small magnitudes and short durations [4], which make them even more difficult to detect than incipient faults. Moreover, system dynamics and multi-level closed-loop control make industrial data autocorrelated. Due to the high-speed sampling requirement for capturing IFs, the property of non-independence in data is stronger and thus non-ignorable during IFD.

As a result, existing MSPM methods have the following problems that limit their application to IFD. On the one hand, static MSPM methods such as principal components analysis (PCA) and partial least squares (PLS) have been found [21–23] to be inefficient for small shifts, let alone IFs. While their existing moving-average (MA) and moving-window (MW) based extensions such as MA-PCA [21], MA-PLS [22], exponentially weighted MA-PCA/PLS [24], multivariate s -term

sum PCA [25] and MW-HMM [26] are sensitive to small shifts, they cannot handle autocorrelations in data. Several studies [27–29] have indicated that monitoring dynamic data using static MSPM methods has the potential to produce excessive false alarms. On the other hand, dynamic MSPM methods such as dynamic PCA (DPCA) and canonical variate analysis (CVA) consider a time sequence of measurements and can capture process dynamics (i.e. handle autocorrelations). However, time lags are chosen only according to system orders, but not considering the characteristics of IFs (i.e., the fault duration and magnitude). Therefore, they may not gain enough sensitivity to IFs, and their efficiency of detecting intermittent small shifts still needs further study. These issues constitute the main motivations of our present study.

This paper investigates the IFD problem in a stationary Gaussian process. A time window and a weight vector are employed to increase the sensitivity to IFs, and the window length is selected considering the characteristics of IFs. Main contributions of the paper are summarized as follows: 1) A weighted moving average T^2 control chart (WMA-TCC) with stationary Gaussian observations is proposed. Different from existing methods that put equal weight on samples within a time window, WMA-TCC uses correlation (autocorrelation and cross-correlation) information to find an optimal weight vector. 2) The concept of IF detectability is defined and corresponding detectability conditions are provided, which further serve as selection criteria of the optimal weight. 3) The optimal weight is given in the form of a solution to nonlinear equations, whose existence is proven with the help of the Brouwer fixed-point theory. Moreover, the uniqueness of the optimal weight is proven in several special cases. 4) We reveal that the optimal weight possesses a symmetrical structure, and an equal weight scheme is optimal when data are independent, which gives more explanations for the rationality of existing MA-based methods. 5) Comprehensive comparative studies with existing static and dynamic MSPM methods, such as PCA, MA-PCA, DPCA and CVA, are carried out on a numerical example and the benchmark continuous stirred tank reactor (CSTR) process, which illustrate the superior IFD performance of the WMA-TCC.

The remainder of this paper is organized as follows. In Section 2, the WMA-TCC with stationary Gaussian observations is introduced for the IFD problem. Then, the detectability of IFs by the WMA-TCC is analyzed in Section 3. The detectability conditions are further utilized to determine the optimal weight in Section 4. Simulation results are presented in Section 5, and con-

clusions are given in Section 6.

Notation: Except where otherwise stated, the notations used throughout the paper are standard. $\mathbb{N}_p(\mu, \Sigma)$ represents a p -dimensional normal distribution with expectation μ and covariance matrix Σ . $\mathbb{W}_p(N, \Sigma)$ represents a p -dimensional Wishart distribution with N degrees of freedom. $\mathbb{F}(p, N - p)$ is a central F distribution with p and $N - p$ degrees of freedom. $\mathbb{F}_\alpha(p, N - p)$ is the $1 - \alpha$ percentile of the central F distribution with p and $N - p$ degrees of freedom. \mathbb{R}^n and $\mathbb{R}^{n \times m}$ denote the n -dimensional Euclidean space and the set of all $n \times m$ real matrices. $\|\xi\|$ and $\|\xi\|_\infty$ denote the Euclidean norm and infinity norm of a vector ξ , respectively. A^T , A^{-1} , $|A|$ and $\text{adj}(A)$ stand for the transpose, the inverse, the determinant and the adjoint of a matrix A , respectively. $\nabla_{\vec{a}_W} \mathcal{L}(\vec{a}_W, \lambda)$ is the gradient of \mathcal{L} with respect to \vec{a}_W . $\nabla_{\vec{a}_W}^2 \mathcal{L}(\vec{a}_W, \lambda)$ is the Hessian matrix of \mathcal{L} with respect to \vec{a}_W . Scalars $a_1 \cdots a_W$ form a row vector by $[a_1, a_2, \dots, a_W]$, and form a column vector by $[a_1; a_2; \dots; a_W]$. \triangleq is to give definition. $H_{l,l'}$ or $[H]_{l,l'}$ is an element of matrix H located in the l th row and l' th column. $H_{l,:}$ and $H_{:,l}$ are the l th row and l th column of matrix H , respectively. $\mathcal{T}_{\setminus i,j}$ is the matrix obtained from \mathcal{T} by deleting the row and column containing $\mathcal{T}_{i,j}$. I_p and e_{p_i} denote the p -dimensional identity matrix and its i th column, respectively; $\mathbf{1}_W$ and $\mathbf{0}_W$ denote the W -dimensional column vectors with all of its entries being one and zero, respectively. The symbol \otimes denotes the Kronecker product and δ_{ij} is the Kronecker function. $\lambda_{\min}(\Gamma)$ and $\lambda_{\max}(\Gamma)$ are the minimum and maximum eigenvalues of matrix Γ , respectively. $A < B$ and $A \leq B$ mean that $A - B$ is negative definite and negative semidefinite, respectively.

2. Methodology

In this section, the WMA-TCC is proposed for the purpose of FD in stationary Gaussian processes.

2.1. Preliminaries

The following lemma is the key result regarding Hotelling's T^2 distribution, see [30].

Lemma 1. Let $T^2 = X^T S^{-1} X$, where X and S are independently distributed random variables with $X \sim \mathbb{N}_p(\mu, \Sigma)$ and $NS \sim \mathbb{W}_p(N, \Sigma)$, where $N \geq p$. Then

$$T^2 \sim \frac{Np}{N - p + 1} \mathbb{F}(p, N - p + 1; \epsilon^2), \quad (1)$$

where the noncentrality parameter $\epsilon^2 = \mu^T \Sigma^{-1} \mu$.

2.2. Weighted moving average T^2 control chart

The IFD task with stationary Gaussian observations concerns the analysis of latest W new current process data $X_{k-W+1}^f, \dots, X_{k-1}^f, X_k^f \in \mathbb{R}^p$ at each time k , to determine whether the process is statistically fault-free or not. Different from existing MA- or MW-based MSPM methods [21, 22, 24–26] that ordinarily have independence and identically Gaussian distribution assumptions, we only assume that systems' normal operation follows a stationary Gaussian process whose autocovariance function reduces to nearly zero for large time lags. That is, for all k , $\mathbb{E}(X_k^f) = \mu_f$ and the autocovariance function $\text{Cov}(X_k^f, X_{k-l}^f) = R_l$ depends only on the lag l . Moreover, we have $\|R_l\| \approx 0$ for large l .

To constitute the WMA-TCC, we collect N sets of W consecutive observations $X_i^j \sim \mathbb{N}_p(\mu, R_0)$, $i = 1, 2, \dots, N$, $j = W, W - 1, \dots, 1$ from the stationary Gaussian process as training data, which can represent the statistic characteristics of systems' normal operating conditions. Moreover, $X_{i_1}^{j_1}$ and $X_{i_2}^{j_2}$ are independent and identically distributed for $i_1 \neq i_2$. This can be achieved by taking samples with long enough intervals between different sets, and thus $\lim_{l \rightarrow \infty} \|R_l\| = 0$. Note that in the same set, the sampling rate of training data should be equal to that of current process data. To sum up, the sampling strategy for training data is shown in (2), where $\widetilde{\cdots}$ means a long enough interval.

$$\begin{aligned} & \{X_1^W, X_1^{W-1}, \dots, X_1^1\}, \widetilde{\cdots}, \{X_2^W, X_2^{W-1}, \dots, X_2^1\}, \widetilde{\cdots} \\ & \vdots \\ & \underbrace{\{X_{N-1}^W, X_{N-1}^{W-1}, \dots, X_{N-1}^1\}}_{\{a_W, a_{W-1}, \dots, a_1\}}, \widetilde{\cdots}, \underbrace{\{X_N^W, X_N^{W-1}, \dots, X_N^1\}}_{\{a_W, a_{W-1}, \dots, a_1\}}. \end{aligned} \quad (2)$$

The IFD problem is equivalent to a hypothesis testing problem concerning testing $H_0 : \mu_f = \mu$ versus $H_1 : \mu_f \neq \mu$. Let $\vec{a}_W = [a_1, a_2, \dots, a_W]^T$ be the weight vector. For the WMA-TCC, we put different weights on samples in the time window, as shown in (2) and (3).

$$\cdots, X_{k-W}^f, \underbrace{\{X_{k-W+1}^f, X_{k-W+2}^f, \dots, X_k^f\}}_{\{a_W, a_{W-1}, \dots, a_1\}}, X_{k+1}^f, \cdots \quad (3)$$

In practice, parameters μ_f, μ, R_l are unknown, and we only know the sample means \bar{X}, \bar{X}_k^f and the sample co-

variance matrix \tilde{S}_W instead:

$$\begin{aligned}\tilde{X}_k^f &= \sum_{j=1}^W a_j X_{k-j+1}^f, \quad \tilde{X}_i = \sum_{j=1}^W a_j X_i^j, \quad \tilde{X} = \frac{1}{N} \sum_{i=1}^N \tilde{X}_i, \\ \tilde{S}_W &= \frac{1}{N-1} \sum_{i=1}^N (\tilde{X}_i - \tilde{X})(\tilde{X}_i - \tilde{X})^T, \quad \sum_{j=1}^W a_j = 1.\end{aligned}\quad (4)$$

Here, $\tilde{X}_k^f, \tilde{X}_i, \tilde{X}, \tilde{S}_W$ are abbreviations for $\tilde{X}_k^f(\vec{d}_W), \tilde{X}_i(\vec{d}_W), \tilde{X}(\vec{d}_W), \tilde{S}_W(\vec{d}_W)$ respectively, since they are actually matrix- or vector-valued functions of \vec{d}_W . We also know that the sample means \tilde{X}_k^f, \tilde{X} and the sample covariance matrix \tilde{S}_W are independently distributed, with

$$\begin{aligned}(N-1)\tilde{S}_W &\sim \mathbb{W}_p(N-1, \tilde{\Sigma}_W), \quad \tilde{\Sigma}_W = \sum_{i=1}^W \sum_{j=1}^W a_i a_j R_{i-j}, \\ (\tilde{X}_k^f - \tilde{X}) &\sim \mathbb{N}_p(\mu_f - \mu, \frac{N+1}{N} \tilde{\Sigma}_W),\end{aligned}\quad (5)$$

where $\tilde{\Sigma}_W$ is an abbreviation for $\tilde{\Sigma}_W(\vec{d}_W)$.

According to Lemma 1, the WMA-TCC with window length W , denoted as WMA-TCC(W), with stationary observations at time instance k is then

$$\begin{aligned}\tilde{T}_k^2(W) &= (\tilde{X}_k^f - \tilde{X})^T \tilde{S}_W^{-1} (\tilde{X}_k^f - \tilde{X}) \\ &\sim \frac{p(N+W)(N-1)}{NW(N-p)} \mathbb{F}(p, N-p).\end{aligned}\quad (6)$$

Here, we assume that $\tilde{S}_W(\vec{d}_W)$ is nonsingular for any weight vector $\vec{d}_W \neq 0_W$. Detailed explanations are given in *Assumption 1* and *Proposition 1* of Section 4. For a given significance level α , the process is considered normal at time instance k , i.e., to accept $H_0 : \mu_f = \mu$, if

$$\tilde{T}_k^2(W) \leq \delta^2 = \frac{p(N^2-1)}{N(N-p)} \mathbb{F}_{\alpha}(p, N-p), \quad (7)$$

where δ^2 is the control limit of the WMA-TCC(W). Otherwise, an alarm occurs at time instance k . Inequality (7) gives the acceptance region of the hypothesis testing.

3. Detectability analyses

For the WMA-TCC, the window length and the weight vector are crucial parameters that can directly affect the IFD performance. They should be carefully selected so that the detection capability for IFs is maximized. Thus, in this section, we analyze the IF detectability.

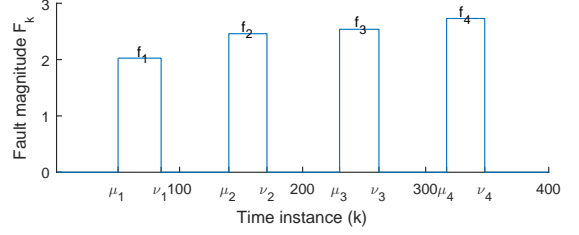


Figure 1: An example of intermittent faults.

3.1. Guaranteed detectability

Consider the following widely used fault model in the MSPM framework [23, 31, 32]:

$$X_k^f = X_k^* + \Xi_k F_k, \quad (8)$$

where X_k^* represents the process fluctuation under normal conditions, Ξ_k is the direction of the fault in time instance k , and F_k is its magnitude. By introducing the time window, we have

$$\tilde{X}_k^f = \tilde{X}_k^* + \tilde{\Xi}_k \tilde{F}_k, \quad \tilde{X}_k^* = \sum_{j=1}^W a_j X_{k-j+1}^*, \quad (9)$$

where $\tilde{\Xi}_k \tilde{F}_k$ is the effect of all faults in the time window, and $\tilde{X}_k^* \sim \mathbb{N}_p(\mu, \tilde{\Sigma}_W)$. When we analyze the fault detectability, we make the following additional assumption:

$$\|\tilde{S}_W^{-1/2}(\tilde{X}_k^* - \tilde{X})\|^2 \leq \delta^2. \quad (10)$$

Remark 1. Inequality (10) is commonly assumed by literature addressing fault detectability problems in the MSPM framework [22, 31–33]. The assumption means that the fault-free process \tilde{X}_k^* fluctuates within its acceptance region (7). Since a small significance level (i.e., $\alpha = 0.01$) is always selected, this assumption holds with high probability. Note that this assumption is only introduced to analyze detectability, and thus has no limitation to the practical application of the method.

In the case of IFs, as shown in Fig. 1, the corresponding fault model can be represented [10, 16, 34] by

$$\Xi_k F_k = \sum_{q=1}^{\infty} [\Gamma(k - \mu_q) - \Gamma(k - \nu_q)] \xi_q f_q, \quad (11)$$

where $\Gamma(\cdot)$ is the step function; μ_q, ν_q represent the appearing and disappearing time of the q th IF, satisfying

$\mu_q < \nu_q < \mu_{q+1}$; and $\xi_q \in \mathbb{R}^p$, $f_q \in \mathbb{R}^1$ are the direction and magnitude of the q th IF, satisfying $\|\xi_q\| = 1$. Moreover, the active and inactive duration of the q th IF are $\tau_q^o = \nu_q - \mu_q$ and $\tau_q^r = \mu_{q+1} - \nu_q$, respectively. Thus, the q th IF can be denoted by five parameters, i.e., $\text{IF}(\xi_q, f_q, \tau_{q-1}^r, \tau_q^o, \tau_q^r)$.

Remark 2. Recall that the characteristics of IFs are small magnitude and short duration. In most cases, since the fault magnitude is small, when an IF becomes active, after exhibiting a short transient behavior, the system will be driven to another steady state soon by the closed-loop control, instead of being continuously sharp fluctuations or out of control. Similarly, when the IF becomes inactive, after a short transition, the closed-loop control will drive the system back to its normal steady state soon. Moreover, since the fault duration is short, we can assume the fault direction and magnitude within each IF to be constant. Therefore, IFs can be represented by the form of intermittent biases as (11). This statement will be confirmed by a realistic simulation of the practical CSTR benchmark in Section 5.

The fault detectability concept was first defined in [35, 36] within the MSPM framework, and has been widely adopted by a variety of MSPM methods [22, 31–33, 37] to study the FD performance. However, the concept has been mainly concerned with PFs. Compared with a PFD task, additional requirements for an IFD [10, 16, 38] are to determine each appearance (disappearance) of an IF before its subsequent disappearance (appearance), otherwise missing or false alarms occur. Following these considerations, this paper extends and generalizes the original fault detectability concept [35] to make it suitable for both PFs and IFs.

Definition 1. For a given significance level α , the disappearance of the q th IF is said to be **guaranteed detectable** (DPG-detectable) by the WMA-TCC(W), if there exists a time instance $\nu_q \leq \mathbf{k}^\# < \mu_{q+1}$ such that for each $\mathbf{k}^\# \leq \mathbf{k} < \mu_{q+1}$, the detection statistic $\tilde{T}_k^2(W) \leq \delta^2$ is guaranteed for all values of \tilde{X}_k^* in (10).

Definition 2. For a given significance level α , the appearance of the q th IF is said to be **guaranteed detectable** (APG-detectable) by the WMA-TCC(W), if the disappearance of the $(q-1)$ th IF is guaranteed detectable, and there exists a time instance $\mu_q \leq \mathbf{k}^* < \nu_q$ such that for each $\mathbf{k}^* \leq \mathbf{k} < \nu_q$, the detection statistic $\tilde{T}_k^2(W) > \delta^2$ is guaranteed for all values of \tilde{X}_k^* in (10).

Definition 3. For a given significance level α , the q th IF is said to be **guaranteed detectable** (G-detectable) by the WMA-TCC(W), if both the q th appearance and disappearance of the IF are guaranteed detectable.

3.2. Detectability conditions

Intuitively, to detect the disappearance/appearance of an IF, we can choose a window length that is no more than the IF's inactive/active duration, so that the WMA-TCC(W) is free from interference of previous faulty/fault-free samples after some delay.

Lemma 2. For the WMA-TCC(W) and a given significance level α , when $W \leq \tau_q^r$, the disappearance of the q th IF is guaranteed detectable (DPG-detectable).

Proof. According to the IF model (11), when $W \leq \tau_q^r$, there exists a time instance $\nu_q \leq \mathbf{k}^\# < \mu_{q+1}$, such that for each $\mathbf{k}^\# \leq \mathbf{k} < \mu_{q+1}$, all W current process samples within the time window are fault-free. Then we have $\tilde{X}_k^f = \tilde{X}_k^*$ and

$$\tilde{T}_k^2(W) = \|\tilde{S}_W^{-1/2}(\tilde{X}_k^f - \tilde{X})\|^2 = \|\tilde{S}_W^{-1/2}(\tilde{X}_k^* - \tilde{X})\|^2.$$

Thus, for each $\mathbf{k}^\# \leq \mathbf{k} < \mu_{q+1}$, the detection statistic $\tilde{T}_k^2(W) \leq \delta^2$ is guaranteed for all values of \tilde{X}_k^* in (10). \square

Lemma 3. For the WMA-TCC(W) and a given significance level α , when $W \leq \min\{\tau_{q-1}^r, \tau_q^o\}$, the appearance of the q th IF is guaranteed detectable (APG-detectable) if and only if

$$\|\tilde{S}_W^{-1/2}\xi_q f_q\| > 2\delta. \quad (12)$$

Proof. According to Lemma 2, when $W \leq \min\{\tau_{q-1}^r, \tau_q^o\}$, the disappearance of the $(q-1)$ th IF is guaranteed detectable. Moreover, there exists a time instance $\mu_q \leq \mathbf{k}^* < \nu_q$, such that for each $\mathbf{k}^* \leq \mathbf{k} < \nu_q$, all W current process samples within the time window are faulty. Then we have $\tilde{X}_k^f = \tilde{X}_k^* + \xi_q f_q$ and

$$\begin{aligned} \tilde{T}_k^2(W) &= \|\tilde{S}_W^{-1/2}(\tilde{X}_k^* - \tilde{X} + \xi_q f_q)\|^2 \\ &\geq \left(\|\tilde{S}_W^{-1/2}\xi_q f_q\| - \|\tilde{S}_W^{-1/2}(\tilde{X}_k^* - \tilde{X})\| \right)^2. \end{aligned} \quad (13)$$

Then by following (12), (10) and (13), we derive that for each $\mathbf{k}^* \leq \mathbf{k} < \nu_q$, $\tilde{T}_k^2(W) > \delta^2$ is guaranteed for all values of \tilde{X}_k^* in (10) and the proof of sufficiency is complete.

We now prove the necessity by contraposition. The contrapositive of the necessity statement is: When $W \leq \min\{\tau_{q-1}^r, \tau_q^o\}$, if $\|\tilde{S}_W^{-1/2}\xi_q f_q\| \leq 2\delta$, then the disappearance of the $(q-1)$ th IF is not guaranteed detectable, or for any time instance $\mu_q \leq \mathbf{k}^* < \nu_q$, there exists a time instance $\mathbf{k}^* \leq \mathbf{k} < \nu_q$ and a value of \tilde{X}_k^* in (10), making $\tilde{T}_k^2(W) \leq \delta^2$ valid. This contrapositive statement can be proven as follows. For any given $\mu_q \leq \mathbf{k}^* < \nu_q$, we consider time instance $k = \nu_q - 1$ which satisfies $\mathbf{k}^* \leq \mathbf{k} < \nu_q$. We further consider the following value

of \tilde{X}_k^* . $\tilde{S}_W^{-1/2}(\tilde{X}_k^* - \tilde{X}) = -\tilde{S}_W^{-1/2}\xi_q f_q/2$, which satisfies (10) if $\|\tilde{S}_W^{-1/2}\xi_q f_q\| \leq 2\delta$. Note that at time instance $k = \nu_q - 1$, we have $\tilde{X}_k^f = \tilde{X}_k^* + \xi_q f_q$ and consequently $\tilde{T}_k^2(W) = \|\tilde{S}_W^{-1/2}\xi_q f_q/2\|^2 \leq \delta^2$. Having proven the contrapositive, we infer the original statement and the proof of necessity is complete. \square

Theorem 1. For the WMA-TCC(W) and a given significance level α , when $W \leq W^\# \triangleq \min\{\tau_{q-1}^r, \tau_q^o, \tau_q^r\}$, the q th IF is guaranteed detectable (G-detectable) if and only if inequality (12) holds.

Proof. Directly derived from Lemmas 2 and 3. \square

4. Determination of the weight and window length

In this section, methods to determine the weight vector and window length are provided, along with discussions on the existence, symmetry and uniqueness of the optimal weight.

4.1. Problem formulation and main results

Now, we are in the position to find the optimal weight vector based on the above derived detectability conditions, and present the main problem as follows.

Problem 1. For the WMA-TCC(W), $W \leq W^\#$, find the optimal weight \vec{a}_W^* that

$$\max_{\vec{a}_W} \beta(\vec{a}_W) = \frac{1}{2} \|\tilde{S}_W^{-1/2}\xi_q\|^2, \quad (14)$$

$$\text{s.t. } g(\vec{a}_W) = \sum_{j=1}^W a_j = 1. \quad (15)$$

Theorem 2. The optimal weight \vec{a}_W^* maximizing $\beta(\vec{a}_W)$ of Problem 1 satisfies

$$\hat{\mathcal{T}}(\vec{a}_W^*)\vec{a}_W^* = b, \quad (16)$$

and

$$(-1)^k |\overline{\mathcal{H}}_k(\vec{a}_W^*)| \geq 0, \quad k = 2, 3, \dots, W, \quad (17)$$

where $\hat{\mathcal{T}}(\vec{a}_W) \in \mathbb{R}^{W \times W}$, $b = [0, \dots, 0, 1]^T \in \mathbb{R}^W$,

$$\hat{\mathcal{T}}_{l,j}(\vec{a}_W) = \begin{cases} \xi_q^T \tilde{S}_W^{-1} (\hat{R}_{lj} - \hat{R}_{(l+1)j}) \tilde{S}_W^{-1} \xi_q, & l < W, \\ 1, & l = W. \end{cases}$$

$$\hat{R}_{lj} = \frac{1}{N-1} \sum_{i=1}^N (X_i^l - \bar{X}^l)(X_i^j - \bar{X}^j)^T,$$

$$\bar{X}^j = \frac{1}{N} \sum_{i=1}^N X_i^j, \quad (18)$$

and \tilde{S}_W is short for $\tilde{S}_W(\vec{a}_W)$ calculated by (4),

$$\left| \overline{\mathcal{H}}_k(\vec{a}_W) \right| = \begin{vmatrix} 0 & 1 & \cdots & 1 \\ 1 & \hat{H}_{1,1}(\vec{a}_W) & \cdots & \hat{H}_{1,k}(\vec{a}_W) \\ \vdots & \vdots & \ddots & \vdots \\ 1 & \hat{H}_{k,1}(\vec{a}_W) & \cdots & \hat{H}_{k,k}(\vec{a}_W) \end{vmatrix},$$

$$\hat{H}_{l,l'}(\vec{a}_W) = h_l^T h_{l'} - \xi_q^T \tilde{S}_W^{-1} \hat{R}_{ll'} \tilde{S}_W^{-1} \xi_q,$$

$$\hat{h}_l(\vec{a}_W) = \tilde{S}_W^{-1/2} \left(\sum_{j=1}^W a_j (\hat{R}_{lj} + \hat{R}_{lj}^T) \right) \tilde{S}_W^{-1} \xi_q. \quad (19)$$

Proof. For this nonlinear constrained optimization problem, we can construct a Lagrange function given by

$$\mathcal{L}(\vec{a}_W, \lambda) = \frac{1}{2} \|\tilde{S}_W^{-1/2}\xi_q\|^2 + \lambda \left(\sum_{j=1}^W a_j - 1 \right), \quad (20)$$

where λ is a Lagrange multiplier. According to the Karush-Kuhn-Tucker conditions (first-order necessary conditions) [39], the optimal weight \vec{a}_W^* should satisfy

$$\nabla_{\vec{a}_W} \mathcal{L}(\vec{a}_W, \lambda) = 0_W, \quad \nabla_{\lambda} \mathcal{L}(\vec{a}_W, \lambda) = 0. \quad (21)$$

Note that

$$\frac{\partial \mathcal{L}(\vec{a}_W, \lambda)}{\partial a_l} = -\frac{1}{2} \xi_q^T \tilde{S}_W^{-1} \left(\frac{\partial \tilde{S}_W}{\partial a_l} \right) \tilde{S}_W^{-1} \xi_q + \lambda$$

$$= -\xi_q^T \tilde{S}_W^{-1} \left(\sum_{j=1}^W a_j \hat{R}_{lj} \right) \tilde{S}_W^{-1} \xi_q + \lambda. \quad (22)$$

By setting the above derivative of $\mathcal{L}(\vec{a}_W, \lambda)$ with respect to \vec{a}_W to zeros, the following equations can be obtained.

$$\xi_q^T \tilde{S}_W^{-1} \left(\sum_{j=1}^W a_j (\hat{R}_{lj} - \hat{R}_{l'j}) \right) \tilde{S}_W^{-1} \xi_q = 0, \quad 1 \leq l, l' \leq W. \quad (23)$$

Thus, integrating (23) with (15), the first-order necessary conditions for the constrained optimization problem are derived as (16).

When \vec{a}_W^* meets (16), it is considered an extremum point or saddle point for function (14) subject to constraint (15). According to [40], second-order necessary conditions for \vec{a}_W^* to be a maximum point are: the leading principal minors of $\overline{\mathcal{H}}(\vec{a}_W^*)$ of order $k+1$ ($k=2, 3, \dots, W$) have sign $(-1)^k$ or equal to zero, where

$$\overline{\mathcal{H}}(\vec{a}_W) = \begin{bmatrix} 0 & \nabla_{\vec{a}_W}^T g(\vec{a}_W) \\ \nabla_{\vec{a}_W} g(\vec{a}_W) & \hat{H}(\vec{a}_W) \end{bmatrix}, \quad (24)$$

is a bordered Hessian matrix and

$$\hat{H}(\vec{a}_W) = \nabla_{\vec{a}_W}^2 \mathcal{L}(\vec{a}_W, \lambda), \text{ i.e. } \hat{H}_{l,r}(\vec{a}_W) = \frac{\partial^2 \mathcal{L}(\vec{a}_W, \lambda)}{\partial a_l \partial a_r}.$$

Thus, the second-order necessary conditions for the optimization problem are derived as (17). \square

4.2. Existence of the solution

In this subsection, we prove the existence of the solution of nonlinear equations (16) with the help of the well-known Brouwer fixed-point theory. We begin with the following assumption and the result is given in *Theorem 3* at last. Additionally, methods to obtain the optimal weight are discussed and a bound of the optimal weight is given.

Assumption 1. $\hat{\Gamma}^W$ is nonsingular, where

$$\hat{\Gamma}^k = \begin{bmatrix} \hat{R}_{11} & \hat{R}_{12} & \cdots & \hat{R}_{1k} \\ \hat{R}_{21} & \hat{R}_{22} & \cdots & \hat{R}_{2k} \\ \vdots & \vdots & \ddots & \vdots \\ \hat{R}_{k1} & \hat{R}_{k2} & \cdots & \hat{R}_{kk} \end{bmatrix} \in \mathbb{R}^{pk \times pk}. \quad (25)$$

Remark 3. *Assumption 1 is the same as the assumption for Yule-Walker equations, which are well-known in the field of parameter identification of time series models. In real applications, Assumption 1 holds due to the existence of process and measurement noises.*

Proposition 1. *Suppose Assumption 1 holds, then $\tilde{S}_W(\vec{a}_W)$ and $\hat{\mathcal{F}}(\vec{a}_W)$ are nonsingular for any $\vec{a}_W \neq 0_W$.*

Proof. By following a few reformulations, we have

$$\tilde{S}_W = \sum_{i=1}^W \sum_{j=1}^W a_i a_j \hat{R}_{ij} = (\vec{a}_W \otimes I_p)^T \hat{\Gamma}^W (\vec{a}_W \otimes I_p). \quad (26)$$

For any $\vec{a}_W \neq 0_W$, the matrix $\vec{a}_W \otimes I_p$ is full column rank. Then, by following *Assumption 1*, we know that $\tilde{S}_W(\vec{a}_W)$ is nonsingular. Let $\hat{\gamma}^W \in \mathbb{R}^{W \times W}$ be the abbreviation of $\hat{\gamma}^W(\vec{a}_W)$, and define

$$\hat{\gamma}_{l,j}^W = \xi_q^T \tilde{S}_W^{-1} \hat{R}_{lj} \tilde{S}_W^{-1} \xi_q. \quad (27)$$

Then, it follows from *Assumption 1* that

$$\hat{\gamma}^W = (I_W \otimes \tilde{S}_W^{-1} \xi_q)^T \hat{\Gamma}^W (I_W \otimes \tilde{S}_W^{-1} \xi_q),$$

is nonsingular and positive definite. By following a few

reformulations, we can rewrite $\hat{\mathcal{F}}(\vec{a}_W) = \hat{J} \hat{\gamma}^W$, where

$$\hat{J} = \begin{bmatrix} 1 & -1 & 0 & \cdots & 0 \\ 0 & 1 & -1 & \ddots & \vdots \\ \vdots & \ddots & \ddots & \ddots & 0 \\ 0 & \cdots & 0 & 1 & -1 \\ \hline & & & & 1_W^T (\hat{\gamma}^W)^{-1} \end{bmatrix} \in \mathbb{R}^{W \times W}.$$

Thus, $\hat{\mathcal{F}}(\vec{a}_W)$ is nonsingular if and only if \hat{J} is nonsingular. We assume that \hat{J} is singular, then there exists $\vec{a}_W = [\alpha_1, \alpha_2, \dots, \alpha_W]^T \neq 0_W$, such that

$$\alpha_1 \hat{J}_{1,:} + \alpha_2 \hat{J}_{2,:} + \cdots + \alpha_{W-1} \hat{J}_{W-1,:} + \alpha_W \hat{J}_{W,:} = 0_W^T.$$

Multiplying both sides by 1_W on the right, we have $\alpha_W 1_W^T (\hat{\gamma}^W)^{-1} 1_W = 0$. Since $\hat{\gamma}^W$ is positive definite, we obtain $\alpha_W = 0$. This means that the first $W - 1$ rows of \hat{J} are linearly dependent, which contradicts the fact that $\hat{J}_{W \setminus \emptyset}$ has full row rank. Thus, \hat{J} is nonsingular and the proof is complete. \square

Remark 4. *According to Proposition 1, we can rewrite*

$$\vec{a}_W^* = \hat{\mathcal{F}}^{-1}(\vec{a}_W^*) b \triangleq \hat{\mathcal{F}}(\vec{a}_W^*) \in \mathbb{R}^W. \quad (28)$$

It can be seen that \vec{a}_W^ is a fixed-point of function $\hat{\mathcal{F}}$. According to our practical experience, \vec{a}_W^* can be obtained by successive approximations within 1000 iterations as follows*

$$\vec{a}_W^{k+1} = \hat{\mathcal{F}}(\vec{a}_W^k), \quad \forall \vec{a}_W^0 \neq 0_W. \quad (29)$$

Since $\hat{\mathcal{F}}(\vec{a}_W) \neq 0_W$, Proposition 1 further guarantees this process is always implementable.

Lemma 4. *For any column vectors x, y and matrix $P \geq 0$, the following inequality holds:*

$$2\|x^T P y\| \leq x^T P x + y^T P y. \quad (30)$$

Proof. Directly derived from $0 \leq (x - y)^T P (x - y)$ and $0 \leq (x + y)^T P (x + y)$. \square

Proposition 2. *Suppose Assumption 1 holds, then $\|\hat{\mathcal{F}}(\vec{a}_W)\|_\infty \leq \frac{W+1}{2W} \frac{\lambda_{\max}(\hat{\Gamma}^W)}{\lambda_{\min}(\hat{\Gamma}^W)} \triangleq d_W$ and $g(\hat{\mathcal{F}}(\vec{a}_W)) = 1$, for any $\vec{a}_W \neq 0_W$.*

Proof. Let $\vec{c}_W = [c_1, \dots, c_W]^T$, according to (28), we have

$$\hat{\mathcal{F}}(\vec{a}_W) = |\hat{\mathcal{F}}(\vec{a}_W)|^{-1} \text{adj}(\hat{\mathcal{F}}(\vec{a}_W)) b = |\hat{\mathcal{F}}(\vec{a}_W)|^{-1} \vec{c}_W, \quad (31)$$

with $c_i = (-1)^{W+i} |\hat{\mathcal{F}}_{\setminus W \setminus i}(\vec{d}_W)| = (-1)^{W+i} |\check{\mathcal{F}}(\vec{d}_W, i)|$, where

$$\check{\mathcal{F}}_{l,j}(\vec{d}_W, i) = \begin{cases} \hat{\mathcal{T}}_{l,j}(\vec{d}_W), & l < W, \\ \delta_{ij}, & l = W. \end{cases} \quad (32)$$

Note that $g(\vec{c}_W) = |\hat{\mathcal{F}}(\vec{d}_W)|$. Thus, $g(\hat{\mathcal{F}}(\vec{d}_W)) = |\hat{\mathcal{F}}(\vec{d}_W)|^{-1} g(\vec{c}_W) = 1$. Moreover, by following a few reformulations, we can rewrite $\check{\mathcal{F}}(\vec{d}_W, i) = \check{J}^i \hat{\gamma}^W$, where

$$\check{J}^i = \begin{bmatrix} 1 & -1 & 0 & \cdots & 0 \\ 0 & 1 & -1 & \ddots & \vdots \\ \vdots & \ddots & \ddots & \ddots & 0 \\ 0 & \cdots & 0 & 1 & -1 \end{bmatrix} \in \mathbb{R}^{W \times W}.$$

$$\frac{e_{W_i}^T (\hat{\gamma}^W)^{-1}}{e_{W_i}^T (\hat{\gamma}^W)^{-1}}$$

Note that $0 < \lambda_{\min}(\hat{\Gamma}^W) I_{pW} \leq \hat{\Gamma}^W \leq \lambda_{\max}(\hat{\Gamma}^W) I_{pW}$. Then

$$0 < \lambda_{\min}(\hat{\Gamma}^W) \varrho(\vec{d}_W) I_W \leq \hat{\gamma}^W \leq \lambda_{\max}(\hat{\Gamma}^W) \varrho(\vec{d}_W) I_W,$$

where $\varrho(\vec{d}_W) = \xi_q^T \tilde{S}_W^{-2} \xi_q$. For $|\hat{J}|$ and $|\check{J}^i|$, adding its j th column to its $j-1$ th column in turn, we obtain $|\hat{J}| = 1_W^T (\hat{\gamma}^W)^{-1} 1_W$ and $|\check{J}^i| = e_{W_i}^T (\hat{\gamma}^W)^{-1} 1_W$. Note that

$$\frac{W}{\lambda_{\max}(\hat{\Gamma}^W) \varrho(\vec{d}_W)} \leq |\hat{J}| = 1_W^T (\hat{\gamma}^W)^{-1} 1_W \leq \frac{W}{\lambda_{\min}(\hat{\Gamma}^W) \varrho(\vec{d}_W)},$$

$$\frac{1}{\lambda_{\max}(\hat{\Gamma}^W) \varrho(\vec{d}_W)} \leq e_{W_i}^T (\hat{\gamma}^W)^{-1} e_{W_i} \leq \frac{1}{\lambda_{\min}(\hat{\Gamma}^W) \varrho(\vec{d}_W)}.$$

Then, according to Lemma 4, we have

$$\|c_i\| = \|\check{J}^i\| |\hat{\gamma}^W| \leq \frac{1}{2} (e_{W_i}^T (\hat{\gamma}^W)^{-1} e_{W_i} + |\hat{J}|) |\hat{\gamma}^W|$$

$$\leq \frac{W+1}{2\lambda_{\min}(\hat{\Gamma}^W) \varrho(\vec{d}_W)} |\hat{\gamma}^W|.$$

For the i th element of $\hat{\mathcal{F}}(\vec{d}_W)$, we have

$$\|\hat{\mathcal{F}}_i(\vec{d}_W)\| = \frac{\|c_i\|}{|\hat{J}| |\hat{\gamma}^W|} \leq \frac{W+1}{2W} \frac{\lambda_{\max}(\hat{\Gamma}^W)}{\lambda_{\min}(\hat{\Gamma}^W)}.$$

Note that $\|\hat{\mathcal{F}}(\vec{d}_W)\|_{\infty} = \max_{i=1, \dots, W} \|\hat{\mathcal{F}}_i(\vec{d}_W)\|$, then the proof is complete. \square

Remark 5. Proposition 2 presents a bound of the optimal weight, i.e., $\vec{d}_W^* \in \mathcal{M}_W$ given in (33). Moreover, Proposition 2 further guarantees the iteration process (29) is always bounded. In the following, we give the well-known Brouwer fixed-point theorem.

Lemma 5. [41] Suppose that M is a nonempty, convex, compact subset of \mathbb{R}^n , where $n \geq 1$, and that $\mathcal{F} : M \rightarrow$

M is a continuous mapping. Then \mathcal{F} has a fixed point.

Theorem 3. Suppose Assumption 1 holds, then the nonlinear equations (16) have a solution.

Proof. Define a subset of \mathbb{R}^W as

$$\mathcal{M}_W = \{\vec{d}_W \in \mathbb{R}^W : g(\vec{d}_W) = 1, \|\vec{d}_W\|_{\infty} \leq d_W\}, \quad (33)$$

and let $\vec{d}_W^x, \vec{d}_W^y \in \mathcal{M}_W$. Then for any $0 \leq \theta \leq 1$, we have $\vec{d}_W^z = \theta \vec{d}_W^x + (1-\theta) \vec{d}_W^y \in \mathcal{M}_W$, which means the set \mathcal{M}_W is convex. This can be seen by

$$g(\vec{d}_W^z) = \theta g(\vec{d}_W^x) + (1-\theta) g(\vec{d}_W^y) = 1,$$

$$\|\vec{d}_W^z\|_{\infty} \leq \theta \|\vec{d}_W^x\|_{\infty} + (1-\theta) \|\vec{d}_W^y\|_{\infty} \leq d_W.$$

Since \mathcal{M}_W is closed and bounded in the finite dimensional normed space \mathbb{R}^W , it is compact. Moreover, for any $\vec{d}_W^0 \in \mathcal{M}_W$, $\hat{\mathcal{F}}(\vec{d}_W) \rightarrow \hat{\mathcal{F}}(\vec{d}_W^0)$ as $\vec{d}_W \rightarrow \vec{d}_W^0$. Thus, $\hat{\mathcal{F}}(\vec{d}_W)$ is continuous on \mathcal{M}_W . According to Proposition 2, we have $\hat{\mathcal{F}}(\mathcal{M}_W) \subseteq \mathcal{M}_W$, where $\hat{\mathcal{F}}(\mathcal{M}_W)$ is the images of \mathcal{M}_W . Now $\hat{\mathcal{F}}$ is a continuous map of the nonempty, convex, compact set \mathcal{M}_W into itself. By Lemma 5, there exists a fixed point for $\hat{\mathcal{F}}$ and consequently the nonlinear equations (16) have a solution. \square

4.3. Symmetry of the optimal weight

Intuitively, since the process is assumed to be stationary, the first and last samples in a time window always have the same contributions to the covariance matrix $\tilde{\Sigma}_W$, as can be seen in (5). Therefore, they should have the same weight when N is sufficiently large. This is also true for the second and the penultimate samples, and so on. In this subsection, we reveal that the optimal weight possesses a symmetrical structure, see Theorem 4.

Proposition 3. When N is sufficiently large, we have

$$\mathbb{E}(\hat{R}_{lj}) = R_{l-j}, \quad \lim_{N \rightarrow \infty} \hat{R}_{lj} = R_{l-j}, \text{ a.s.} \quad (34)$$

$$\mathbb{E}(\tilde{S}_W) = \tilde{\Sigma}_W, \quad \lim_{N \rightarrow \infty} \tilde{S}_W = \tilde{\Sigma}_W, \text{ a.s.} \quad (35)$$

Proof. According to (26), we can derive (35) directly if (34) holds. As for (34), note that $X_{i_1}^{j_1}$ and $X_{i_2}^{j_2}$ are independent for $i_1 \neq i_2$. Thus, $\mathbb{E}(X_{i_1}^{j_1} (\bar{X}^{j_1})^T) = \mathbb{E}(\bar{X}^{j_1} (X_{i_1}^{j_1})^T) = \frac{1}{N} R_{l-j} + \mu \mu^T$ and $\mathbb{E}(\bar{X}^{j_1} (\bar{X}^{j_2})^T) = \frac{1}{N} R_{l-j} + \mu \mu^T$. Then

$$\mathbb{E}(\hat{R}_{lj}) = \frac{1}{N-1} \sum_{i=1}^N \mathbb{E}(X_i^l (X_i^j)^T - X_i^l (\bar{X}^j)^T - \bar{X}^l (X_i^j)^T + \bar{X}^l (\bar{X}^j)^T) = R_{l-j}.$$

Moreover, it is well known that the stationary Gaussian process is ergodic. Thus,

$$\lim_{N \rightarrow \infty} \bar{X}^j = \lim_{N \rightarrow \infty} \frac{1}{N} \sum_{i=1}^N X_i^j = \mathbb{E}(X_i^j) = \mu, \text{ a.s.},$$

$$\lim_{N \rightarrow \infty} \frac{1}{N-1} \sum_{i=1}^N X_i^l (X_i^j)^T = \mathbb{E}(X_i^l (X_i^j)^T) = R_{l-j} + \mu \mu^T, \text{ a.s.}$$

Substituting them into (18), we derive (34). \square

Theorem 4. *Suppose Assumption 1 holds and N is sufficient large, then the optimal weight \vec{a}_W^* maximizing $\beta(\vec{a}_W)$ of Problem 1 satisfies*

$$a_j^* = a_{W-j+1}^*, \quad 1 \leq j \leq W. \quad (36)$$

Proof. According to Proposition 3, when N is sufficiently large, we almost surely have

$$\mathcal{T}_{l,j} = \begin{cases} \xi_q^T \tilde{\Sigma}_W^{-1} (R_{l-j} - R_{l+1-j}) \tilde{\Sigma}_W^{-1} \xi_q, & l < W, \\ 1, & l = W, \end{cases}$$

where \mathcal{T} is short for $\mathcal{T}(\vec{a}_W)$, such that

$$\mathcal{T}(\vec{a}_W^*) \vec{a}_W^* = b.$$

Following $R_{-l} = R_l^T$, it can be seen that

$$\begin{aligned} \mathcal{T}_{l,j} &= \mathcal{T}_{l+1,j+1}, & l < W-1, j < W, \\ \mathcal{T}_{l,j} &= -\mathcal{T}_{j-1,l}, & l \leq W-1, j \leq W. \end{aligned}$$

Denote $A_{\setminus l \setminus \emptyset}$ and $A_{\setminus \emptyset \setminus j}$ as the matrices obtained from A by deleting the l th row and j th column, respectively. Then, $\mathcal{T}_{\setminus W \setminus \emptyset} \in \mathbb{R}^{W-1 \times W}$ has the following form

$$\mathcal{T}_{\setminus W \setminus \emptyset} = \begin{bmatrix} -t_1 & t_1 & t_2 & \cdots & t_{W-2} & t_{W-1} \\ -t_2 & -t_1 & t_1 & t_2 & \ddots & t_{W-2} \\ -t_3 & -t_2 & -t_1 & t_1 & \ddots & \vdots \\ \vdots & \ddots & \ddots & \ddots & \ddots & t_2 \\ -t_{W-1} & \cdots & -t_3 & -t_2 & -t_1 & t_1 \end{bmatrix},$$

where $t_l = \xi_q^T \tilde{\Sigma}_W^{-1} (R_{-l} - R_{l-1}) \tilde{\Sigma}_W^{-1} \xi_q$. Define $\text{cen}(A) \in \mathbb{R}^{m \times n}$ as the centrosymmetry of a matrix $A \in \mathbb{R}^{m \times n}$, namely, $[\text{cen}(A)]_{l,j} = [A]_{m-l+1, n-j+1}$. It can be easily verified that the operator $\text{cen}()$ has the following properties:

$$\text{cen}(\text{cen}(A)) = A, \quad \text{cen}(-A) = -\text{cen}(A). \quad (37)$$

Besides, if A is a square matrix, then we have $|\text{cen}(A)| = |A|$. Moreover, if A is centrosymmetric, that is to say,

$\text{cen}(A) = A$, then we have

$$\text{cen}(A_{\setminus \emptyset \setminus j}) = A_{\setminus \emptyset \setminus n-j+1}. \quad (38)$$

Note that $[\mathcal{T}_{\setminus W \setminus \emptyset}]_{l,j} = -[\mathcal{T}_{\setminus W \setminus \emptyset}]_{W-l, W-j+1}$, i.e. $\text{cen}(\mathcal{T}_{\setminus W \setminus \emptyset}) = -\mathcal{T}_{\setminus W \setminus \emptyset}$. According to (37) and (38), we have

$$\text{cen}(\mathcal{T}_{\setminus W \setminus j}) = -\mathcal{T}_{\setminus W \setminus W-j+1}. \quad (39)$$

Thus,

$$|\mathcal{T}_{\setminus W \setminus j}| = |-\text{cen}(\mathcal{T}_{\setminus W \setminus W-j+1})| = (-1)^{W-1} |\mathcal{T}_{\setminus W \setminus W-j+1}|.$$

Since $\mathcal{T}(\vec{a}_W)$ is nonsingular for any weight vector $\vec{a}_W \neq 0_W$, similar to the Cramer's rule, we have $\vec{a}_W^* = \mathcal{T}^{-1}(\vec{a}_W^*) b = |\mathcal{T}(\vec{a}_W^*)|^{-1} \text{adj}(\mathcal{T}(\vec{a}_W^*)) b$. Then

$$\begin{aligned} a_j^* &= (-1)^{W+j} |\mathcal{T}(\vec{a}_W^*)|^{-1} |\mathcal{T}_{\setminus W \setminus j}(\vec{a}_W^*)| \\ &= (-1)^{2W-j+1} |\mathcal{T}(\vec{a}_W^*)|^{-1} |\mathcal{T}_{\setminus W \setminus W-j+1}(\vec{a}_W^*)| = a_{W-j+1}^*, \end{aligned}$$

which completes the proof. \square

4.4. Further results in several special cases

Note that Theorem 2 only gives the necessary conditions. Nevertheless, in some special cases, we can further find necessary and sufficient conditions, and determine the optimal weight exactly.

Proposition 4. *If \vec{a}_W^* meets (16) and makes the strict inequality in (17) hold, then it is the optimal weight maximizing $\beta(\vec{a}_W)$ of Problem 1.*

Proof. According to [40], when \vec{a}_W^* meets the first-order necessary conditions (16), the second-order sufficient conditions for \vec{a}_W^* to be a maximum point (rather than a minimum or saddle point) are: the leading principal minors of $\overline{\mathcal{H}}(\vec{a}_W^*)$ of order $k+1$ ($k=2, 3, \dots, W$) have sign $(-1)^k$. By following Theorem 2, we obtain this proposition. \square

Proposition 5. *For the optimal weight \vec{a}_W^* maximizing $\beta(\vec{a}_W)$ of Problem 1, we have*

$$2\beta(\vec{a}_W^*) = \hat{\gamma}_{l:}^W(\vec{a}_W^*) \vec{a}_W^*, \quad 1 \leq l \leq W. \quad (40)$$

Proof. It follows from (26) that

$$\begin{aligned} \|\tilde{\mathcal{S}}_W^{-1/2} \xi_q\|^2 &= \xi_q^T \tilde{\mathcal{S}}_W^{-1} (\vec{a}_W \otimes I_p)^T \hat{\Gamma}_W (\vec{a}_W \otimes I_p) \tilde{\mathcal{S}}_W^{-1} \xi_q \\ &= (\vec{a}_W \otimes \tilde{\mathcal{S}}_W^{-1} \xi_q)^T \hat{\Gamma}_W (\vec{a}_W \otimes \tilde{\mathcal{S}}_W^{-1} \xi_q) \\ &= \vec{a}_W^T (I_W \otimes \tilde{\mathcal{S}}_W^{-1} \xi_q)^T \hat{\Gamma}_W (I_W \otimes \tilde{\mathcal{S}}_W^{-1} \xi_q) \vec{a}_W = \vec{a}_W^T \hat{\gamma}^W \vec{a}_W. \end{aligned}$$

Note that we have $\hat{\gamma}_{l,:}^W(\vec{a}_W^*)\vec{a}_W^* = \hat{\gamma}_{l,:}^W(\vec{a}_W^*)\vec{a}_W^*$ from (16). Thus,

$$\begin{aligned} 2\beta(\vec{a}_W^*) &= \|\tilde{S}_W^{-1/2}(\vec{a}_W^*)\xi_q\|^2 = (\vec{a}_W^*)^T \hat{\gamma}^W(\vec{a}_W^*) \\ &= (\vec{a}_W^*)^T [\hat{\gamma}_{:,1}^W(\vec{a}_W^*), \dots, \hat{\gamma}_{:,l}^W(\vec{a}_W^*)] \vec{a}_W^* = (\vec{a}_W^*)^T \hat{\gamma}_{:,l}^W(\vec{a}_W^*). \end{aligned}$$

The last equality is because $1_{l,W}^T \vec{a}_W^* = 1$. Then by following $(\hat{\gamma}_{:,l}^W)^T = \hat{\gamma}_{l,:}^W$, we obtain (40). \square

Theorem 5. *When process data are independent, R_0 is nonsingular and N is sufficiently large, the optimal weight \vec{a}_W^* maximizing $\beta(\vec{a}_W)$ of Problem 1 is uniquely determined as*

$$a_1^* = a_2^* = \dots = a_W^* = 1/W. \quad (41)$$

Proof. When process data are independent, we have $R_l = 0, \forall l \neq 0$. By following the proof of *Theorem 4*, when N is sufficiently large, we almost surely have

$$\mathcal{T}(\vec{a}_W) = \begin{bmatrix} t_0 & -t_0 & 0 & \dots & 0 \\ 0 & t_0 & -t_0 & \ddots & \vdots \\ \vdots & \ddots & \ddots & \ddots & 0 \\ 0 & \dots & 0 & t_0 & -t_0 \\ 1 & \dots & 1 & \dots & 1 \end{bmatrix}, \quad (42)$$

where $t_0 = \xi_q^T \tilde{S}_W^{-1} R_0 \tilde{S}_W^{-1} \xi_q > 0$. Note that

$$|\mathcal{T}(\vec{a}_W)| = W(t_0)^{W-1}, \quad |\mathcal{T}_{\setminus W \setminus j}(\vec{a}_W)| = (-1)^{W-j} (t_0)^{W-1}.$$

Thus, $a_j^* = (-1)^{W+j} |\mathcal{T}(\vec{a}_W^*)|^{-1} |\mathcal{T}_{\setminus W \setminus j}(\vec{a}_W^*)| = 1/W$. Then, $\tilde{S}_W(\vec{a}_W^*) = \frac{1}{W} R_0$. Substituting them into (19), we have $\hat{H}_{l,l'}(\vec{a}_W^*) \rightarrow H_{l,l'}(\vec{a}_W^*) = 4W\vartheta - W^2\vartheta\delta_{ll'}$ almost surely when N is sufficiently large, where $\vartheta = \xi_q^T R_0^{-1} \xi_q$. Thus,

$$|\overline{\mathcal{H}}_k(\vec{a}_W^*)| = \begin{vmatrix} 0 & 1_k^T \\ 1_k & -(W^2\vartheta)I_k \end{vmatrix} = k(-1)^k (W^2\vartheta)^{k-1}.$$

Following *Proposition 4*, (41) is the optimal weight. \square

Remark 6. *Theorem 5 explains why the MA scheme with equal weight is always adopted in FD tasks where samples are assumed to be independent, such as in [21, 22, 25, 42].*

Theorem 6. *When $p = 1$, suppose Assumption 1 holds, then the optimal weight \vec{a}_W^* maximizing $\beta(\vec{a}_W)$ of Problem 1 is uniquely determined as*

$$\vec{a}_W^* = \hat{A}^{-1}b, \quad (43)$$

where

$$\hat{A}_{l,j} = \begin{cases} \hat{R}_{lj} - \hat{R}_{(l+1)j}, & l < W, \\ 1, & l = W. \end{cases} \quad (44)$$

Proof. When $p = 1$, we have $\xi_q = 1$, and $\tilde{S}_W(\vec{a}_W)$ is a scalar. Thus, (16) degenerates into linear equations with unique solutions (43). It follows from *Proposition 5* that

$$2\beta(\vec{a}_W^*) = \tilde{S}_W^{-1}(\vec{a}_W^*) = \hat{\gamma}_{l,:}^W(\vec{a}_W^*)\vec{a}_W^*, \quad 1 \leq l \leq W. \quad (45)$$

Multiplying both sides by $\tilde{S}_W^2(\vec{a}_W^*)$ and following (27), we obtain $\tilde{S}_W(\vec{a}_W^*) = \hat{\Gamma}_{l,:}^W(\vec{a}_W^*)$. Substituting it into (19), we have

$$\hat{H}_{l,l'}(\vec{a}_W^*) = 4\tilde{S}_W^{-1}(\vec{a}_W^*) - \tilde{S}_W^{-2}(\vec{a}_W^*)\hat{R}_{ll'},$$

and thus,

$$\begin{aligned} |\overline{\mathcal{H}}_k(\vec{a}_W^*)| &= \begin{vmatrix} 0 & 1_k^T \\ 1_k & \tilde{S}_W^{-2}(\vec{a}_W^*)\hat{\Gamma}^k \end{vmatrix} \\ &= (-1)^k (\tilde{S}_W^2(\vec{a}_W^*)1_k^T (\hat{\Gamma}^k)^{-1} 1_k) |\tilde{S}_W^{-2}(\vec{a}_W^*)\hat{\Gamma}^k|. \end{aligned}$$

Note that $\tilde{S}_W, \hat{\Gamma}^k$ are positive definite, then

$$(-1)^k |\overline{\mathcal{H}}_k(\vec{a}_W^*)| > 0, \quad k = 2, 3, \dots, W.$$

Following *Proposition 4*, (43) is the optimal weight. \square

Theorem 7. *When $W = 2$, suppose Assumption 1 holds and N is sufficiently large, then the optimal weight \vec{a}_W^* maximizing $\beta(\vec{a}_W)$ of Problem 1 is uniquely determined as*

$$a_1^* = a_2^* = 1/2. \quad (46)$$

Proof. When $W = 2$, (46) can be derived directly from *Theorem 4*. When N is sufficiently large, we have

$$\hat{h}_l(\vec{a}_W) \rightarrow h_l(\vec{a}_W) = \tilde{S}_W^{-1/2} \left(\sum_{j=1}^W a_j (R_{l-j} + R_{l-j}^T) \right) \tilde{S}_W^{-1} \xi_q.$$

Note that when $W = 2$, we have $h_1(\vec{a}_2^*) = h_2(\vec{a}_2^*)$. Thus,

$$|\overline{\mathcal{H}}_k(\vec{a}_2^*)| = \begin{vmatrix} 0 & 1_k^T \\ 1_k & -\hat{\gamma}^k \end{vmatrix} = (-1)^k (1_k^T (\hat{\gamma}^k)^{-1} 1_k) |\hat{\gamma}^k|.$$

Following *Proposition 4*, (46) is the optimal weight. \square

Remark 7. *Note that the derived weights (41), (43) and (46) are optimal regardless of the direction of IFs in these three cases, respectively.*

4.5. Selection of the window length

One drawback of introducing a time window is that it causes detection delays. Generally speaking, an over-large window length may incur serious detection delays. As a result, we suggest choosing the smallest window length that guarantees the detection of IFs.

Theorem 8. For the WMA-TCC with $W \leq W^\#$ and a given significance level α , the q th IF is guaranteed detectable (G-detectable) if and only if

$$\beta(\bar{a}_{W^\#}^*)f_q^2 > 2\delta^2. \quad (47)$$

Then the window length W can be chosen such that $W^\# \geq W \geq W^*$, where

$$W^* = \arg \min_W \beta(\bar{a}_W^*)f_q^2 > 2\delta^2. \quad (48)$$

Proof. Note that $\beta([\bar{a}_{W-1}^*; 0]) \leq \beta(\bar{a}_W^*)$. Thus, we can conclude that when $W \leq W^\#$, the maximum of $\beta(\bar{a}_W)$ achieves with $W = W^\#$ and $\bar{a}_W = \bar{a}_{W^\#}^*$. Then, this theorem holds according to *Theorem 1*. \square

In practice, IFs' parameters may not be known exactly, but in most cases lower bounds of fault parameters are available through expert knowledge or analyzing historical data and operating conditions. Denote $\tilde{f}_q, \tilde{\tau}_{q-1}^r, \tilde{\tau}_q^o, \tilde{\tau}_q^r$ as the lower bounds of $f_q, \tau_{q-1}^r, \tau_q^o, \tau_q^r$, respectively. Then we have the following corollaries.

Corollary 1. For the WMA-TCC(W) and a given significance level α , when $W \leq \tilde{W}^\# \triangleq \min\{\tilde{\tau}_{q-1}^r, \tilde{\tau}_q^o, \tilde{\tau}_q^r\}$, the q th IF is guaranteed detectable (G-detectable) if $IF(\xi_q, \tilde{f}_q, \tilde{\tau}_{q-1}^r, \tilde{\tau}_q^o, \tilde{\tau}_q^r)$ is guaranteed detectable.

Proof. Directly derived from *Theorem 1*. \square

Corollary 2. For the WMA-TCC with $W \leq \tilde{W}^\#$ and a given significance level α , the q th IF is guaranteed detectable (G-detectable) if

$$\beta(\bar{a}_{\tilde{W}^\#}^*)\tilde{f}_q^2 > 2\delta^2. \quad (49)$$

Then the window length W can be chosen such that $\tilde{W}^\# \geq W \geq \tilde{W}^*$, where

$$\tilde{W}^* = \arg \min_W \beta(\bar{a}_W^*)\tilde{f}_q^2 > 2\delta^2. \quad (50)$$

Proof. Directly derived from *Theorem 8* and *Corollary 1*. \square

Remark 8. A PF can be viewed as an IF with infinite active duration. Thus, all the above analyses, including all the theorems, propositions and corollaries, are applicable to PF by setting $\tau_{q-1}^r, \tau_q^o, \tau_q^r \rightarrow \infty$.

5. Simulation studies

In this section, two simulation examples are used to demonstrate the efficiency of the WMA-TCC, by comparing with existing static and dynamic MSPM methods.

5.1. A numerical example

A multivariate AR(1) process model used in the original DPCA literature [27] is employed here to illustrate the effectiveness and efficiency of the developed method, in comparison with several well-known methods. The process model under normal operating conditions is

$$\begin{aligned} \mathbf{z}_k &= \begin{bmatrix} 0.118 & -0.191 \\ 0.847 & 0.264 \end{bmatrix} \mathbf{z}_{k-1} + \begin{bmatrix} 1 & 2 \\ 3 & -4 \end{bmatrix} \mathbf{u}_{k-1}, \\ \mathbf{y}_k &= \mathbf{z}_k + \mathbf{v}_k, \end{aligned} \quad (51)$$

where \mathbf{u} is the correlated input:

$$\mathbf{u}_k = \begin{bmatrix} 0.811 & -0.226 \\ 0.477 & 0.415 \end{bmatrix} \mathbf{u}_{k-1} + \begin{bmatrix} 0.193 & 0.689 \\ -0.320 & -0.749 \end{bmatrix} \mathbf{w}_{k-1}.$$

According to [27], the noises \mathbf{w} and \mathbf{v} are zero means, and follow Gaussian distribution with variance 1 and 0.1, respectively. Both \mathbf{u} and \mathbf{y} are measured so that we can form the process data as $X_k = [\mathbf{y}_k; \mathbf{u}_k]$.

Both 5000 sets of 10 consecutive observations (training samples) and 800 consecutive observations (test samples) are generated according to (51), and intermittent process faults are subsequently introduced in the test dataset since sample 401. The first 400 test samples are used to calculate false alarm rates (FARs) of different methods. The introduced IFs have an additive form as modeled by (11) with the fault direction $\xi_q = [0.0319, -0.2740, 0.9611, -0.0098]^T$, the lower bound of each fault magnitude $\tilde{f}_q = 0.42$, the lower bound of each fault active and inactive duration $\tilde{\tau}_q^o = 15, \tilde{\tau}_q^r = 20$. The actual fault magnitude, fault active and inactive duration are all generated randomly according to their lower bounds and are shown in Fig. 2 with a black line (the Y-axis shows the fault magnitude multiplied by 2.3, and the X-axis shows the fault active and inactive duration).

Training samples are used to determine the optimal weight vector and the significance level α is set as 0.01. Then, we can conclude that the introduced IFs are guaranteed detectable by the WMA-TCC with window length $W \in [10, 15]$, according to *Theorems 1* and *8* and *Corollary 2*. The WMA-TCC with window length $W = 10$ is given in Fig. 3 with a red line. To demonstrate

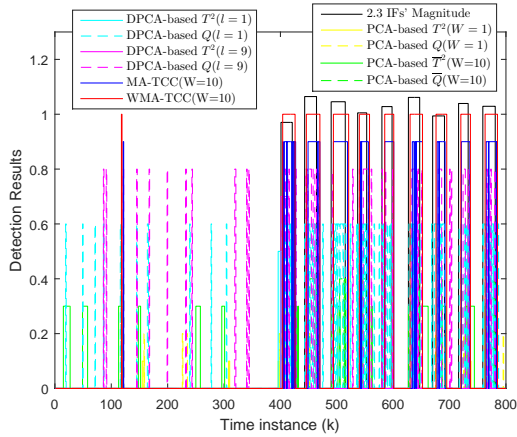


Figure 2: IFD results using different methods in the numerical simulation.

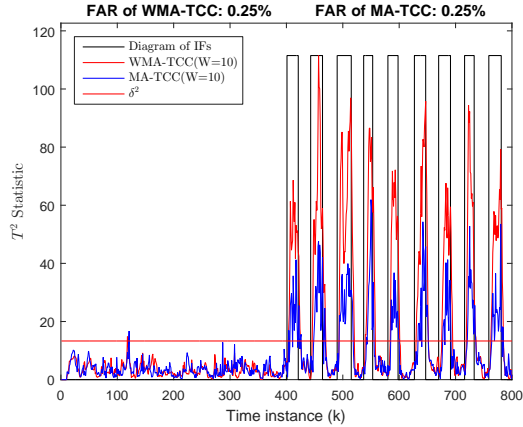


Figure 3: IFD using the WMA-TCC and MA-TCC with window length $W = 10$ in the numerical simulation.

the importance of employing an optimal weight vector, the WMA-TCC with equal weight scheme, denoted here as MA-TCC, with window length $W = 10$ is also given in Fig. 3 for comparison. It is noted that the MA-TCC fluctuates around its control limit whereas the WMA-TCC goes beyond its control limit clearly. This phenomenon can be explained by *Theorem 1*, which says that the introduced IFs are not guaranteed detectable by the MA-TCC(10). Overall, their detailed IFD results are given in Fig. 2 with blue and red lines, respectively.

Several static and dynamic MSPM methods are used here to show their limitations on dealing with IFs. Another 50000 consecutive observations are generated according to (51) as training samples for these MSPM methods. The traditional PCA and its MA-based exten-

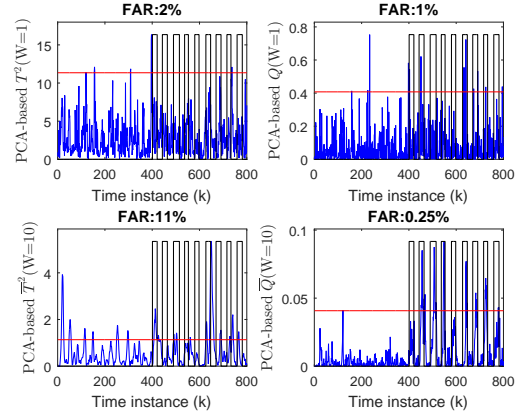


Figure 4: IFD using PCA-based and MA-PCA-based ($W = 10$) control charts in the numerical simulation.

sion (i.e., the MA-PCA [22]), are selected as the representatives of static MSPM methods. For PCA and MA-PCA models, the cumulative percent variance (CPV) criterion says that three PCs should be chosen, which account for more than 95% of the variance in original variables. The MA-PCA-based T^2 and Q statistics with window length $W = 10$, denoted here as PCA-based $\bar{T}^2(10)$ and PCA-based $\bar{Q}(10)$, are utilized for comparison. The PCA-based and MA-PCA-based control charts of the test data are given in Fig. 4. Moreover, their detailed IFD results are given in Fig. 2 with yellow and green lines, respectively. It can be seen that traditional PCA is inefficient for IFs and the MA-PCA has an unacceptable high FAR (11%). This high FAR is expected since several studies [27–29] have already indicated that monitoring autocorrelated data using static MSPM methods tends to produce excessive false alarms.

As for dynamic MSPM methods, we select DPCA [27] as their representative in this subsection, because the simulation model (51) was first introduced therein. According to [27], the time lag is determined as $l = 1$, and five PCs are chosen for the DPCA model. The DPCA-based T^2 and Q statistics of the test data are given in Fig. 5. Moreover, their detailed IFD results are given in Fig. 2 with solid and dashed cyan lines, respectively. It is obvious that the IFD performance of both statistics is far from satisfactory. For further comparison, the time lag is chosen as $l = 9$, so that the same number of samples with WMA-TCC(10), i.e., 10 samples, can be utilized to detect IFs at each time instance. According to the CPV criterion, twelve PCs should be chosen for the DPCA model at this time, which account

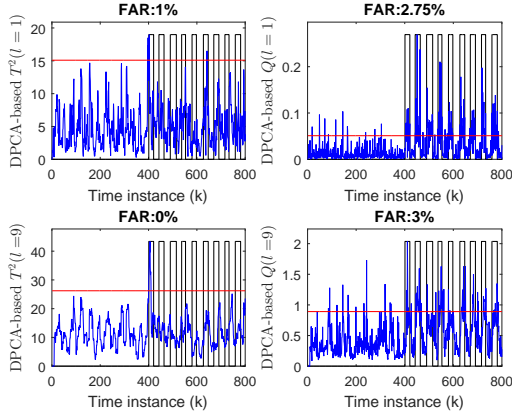


Figure 5: IFD using DPCA-based control charts with time lag $l = 1$ and $l = 9$ in the numerical simulation.

for more than 99% of the variance in original variables. The DPCA-based $T^2(l = 9)$ and $Q(l = 9)$ statistics of the test data are given in Fig. 5, along with their detailed IFD results given in Fig. 2 with solid and dashed magenta lines, respectively. It can be seen that the IFD performance is still unsatisfactory.

To appreciate the performance of different methods, their IFD results are shown together in Fig. 2. It is noted that only WMA-TCC goes beyond its control limit clearly when an IF occurs. By contrast, the others all tend to fluctuate around their corresponding control limits. Thus, it can be seen that the developed method shows the best IFD performance among several static and dynamic MSPM methods.

5.2. The CSTR process

In this subsection, a continuous stirred tank reactor (CSTR) simulation is utilized to demonstrate the effectiveness and efficiency of the proposed methods through comparative studies. The CSTR process can be described by the following differential equations

$$\begin{aligned} \frac{dC_A}{dt} &= \frac{q}{V}(C_{Af} - C_A) - k_0 \exp\left(-\frac{E}{RT}\right)C_A + v_1, \\ \frac{dT}{dt} &= \frac{q}{V}(T_f - T) - \frac{\Delta H}{\rho C_p}k_0 \exp\left(-\frac{E}{RT}\right)C_A + \frac{UA}{V\rho C_p}(T_c - T) + v_2, \end{aligned} \quad (52)$$

where $C_A, T, T_c, q, C_{Af}, T_f$ are the outlet concentration, reactor temperature, cooling water temperature, feed flow rate, feed concentration and feed temperature, respectively. v_1 and v_2 are independent Gaussian white noises. The measured variables are $[C_A, T, T_c, q]^T$, where $[C_A, T]^T$ are controlled variables with nominal values, and $[T_c, q]^T$ are manipulated variables with feedback control. More detailed descriptions of the CSTR

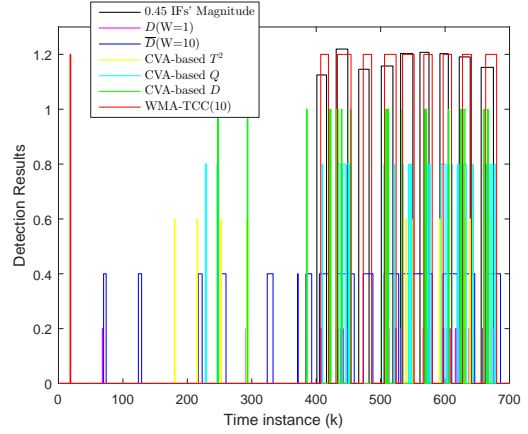


Figure 6: IFD results using different methods in the CSTR process.

process can be found in [43], where the settings of the process, including system parameters and conditions as well as controller information, are also given therein. Different from most existing literature that always sets the sampling interval as 1min (in this situation, process data are nearly independent), we choose the sampling interval as 3s here because of the higher sampling frequency requirement for capturing IFs. Note that shortening the sampling interval results in autocorrelated process data.

The unmeasurable feed temperature T_f is a main disturbance in the process, and has been used by many studies [44, 45] to evaluate different FD methods. In this simulation, intermittent increases of feed temperature T_f are introduced since sample 401, with a lower bound of each fault magnitude $\tilde{f}_q = 2.5\text{K}$, a lower bound of each fault active, and inactive duration $\tilde{\tau}_q^o = \tilde{\tau}_q^r = 10$ sampling times, i.e., 30s. The first 400 samples are used to calculate FARs of different methods. A total of 700 consecutive observations are collected as test samples. The actual fault magnitude, fault active and inactive duration are all generated randomly according to their lower bounds and are shown in Fig. 6 with a black line (the Y-axis shows the fault magnitude multiplied by 0.45, and the X-axis shows the fault active and inactive duration).

According to the process model (52), T_f directly affects the reactor temperature T . However, since T is controlled by manipulating the cooling water temperature T_c , when T deviates from its nominal value, T_c is immediately adjusted to compensate the change. In this way, the entire process is always under control, rendering the system parameters and conditions unchanged. Therefore, when intermittent disturbances of

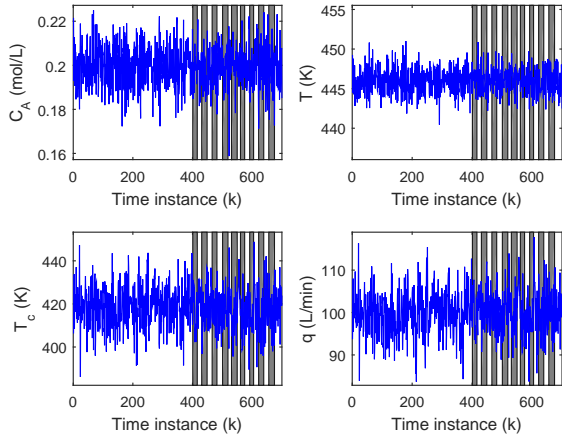


Figure 7: Measured CSTR process variables with intermittent disturbances in the feed temperature T_f .

T_f occur, C_A, T, q are still around their set-point values, whereas T_c exhibits intermittent biases instead. This phenomenon is also shown in Fig. 7, where collected process data with intermittent disturbances in T_f are plotted and the gray shadows represent the active duration of IFs. Moreover, note that the correlations (autocorrelation and cross-correlation) of process variables in this scenario remain unchanged. This can be seen from (52) that time constants of C_A, T are irrelevant with T_f, T_c . As a result, the introduced intermittent disturbances in T_f can be well modeled by (11) with fault direction $\xi_q = [0, 0, 1, 0]^T$.

Five thousand sets of 10 consecutive observations are collected under normal conditions as training samples, which are subsequently utilized to determine the optimal weight vector and the control limit with significance level $\alpha = 0.01$. Then, we can conclude that the introduced intermittent disturbances in T_f are guaranteed detectable by the WMA-TCC with window length $W = 10$, according to *Theorems 1* and *8* and *Corollary 2*. Several well-known static and dynamic MSPM methods are also employed here for comparison. The Mahalanobis distance D (also known as the global Hotelling's T^2 test) [2], and its MA-based extension [22] with window length $W = 10$, i.e., $\bar{D}(10)$, are chosen as representatives of static MSPM methods. As for dynamic MSPM methods, CVA is chosen as their representative. Another 50,000 consecutive observations are collected under normal conditions as training samples for these MSPM methods.

The WMA-TCC(10), $D(1)$ and $\bar{D}(10)$ control charts

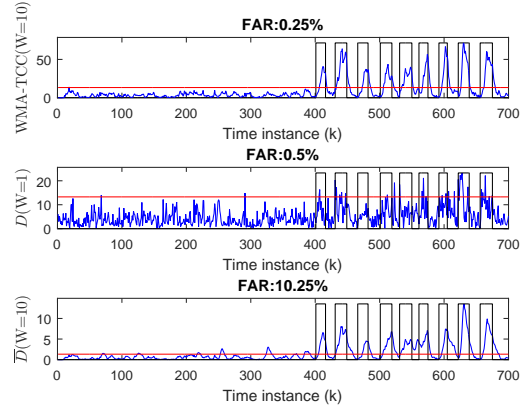


Figure 8: IFD using WMA-TCC, Mahalanobis distance and MA-Mahalanobis distance in the CSTR process.

of the test data are given in Fig. 8. Moreover, their detailed IFD results are given in Fig. 6 with red, magenta and blue lines, respectively. It can be seen that the $D(1)$ statistic is inefficient for IFs. While the traditional MA technique can indeed improve the statistics' sensitivity to IFs, it causes an unacceptable high FAR (10.25%) when process data are autocorrelated, and consequently invalidates the online monitoring approach. By contrast, the proposed WMA-TCC goes beyond its control limit clearly when IFs occur, and the FAR is consistent with its theoretical value, i.e., less than 1%. As for the CVA model, according to [46], the number of time lags for past (p) and future (f) observations is determined using autocorrelation analysis on the training samples. For the simulation, it has been found that three time lags are the maximum, after which autocorrelations become insignificant for the summed squares of all measurements as well as for all the process variables, at 99% confidence level. Thus, we set $p = f = 3$. In addition, the number of states is chosen as four according to the dominant singular value (SV) method (to find the point where a "knee" appears in the SV curve). The CVA-based T^2, Q, D statistics [46] of the test data are given in Fig. 9, and their detailed IFD results are given in Fig. 6 with yellow, cyan and green lines, respectively. The IFD results indicate that CVA also has limitations on dealing with IFs. The time lags of CVA are chosen only based on system dynamics without taking the characteristics of IFs into account, resulting in a lack of sensitivity to IFs of the method.

Finally, to appreciate the performance of different methods, their IFD results are shown together in Fig. 6. It is noted that only WMA-TCC alarms continuously

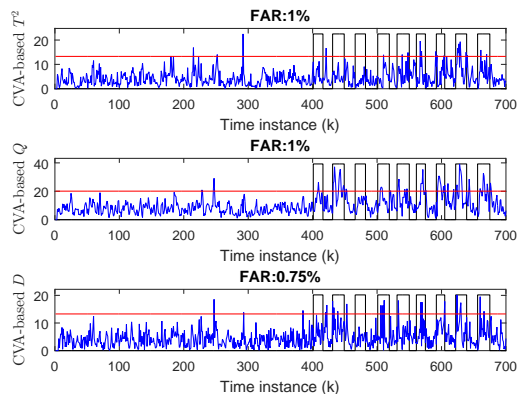


Figure 9: IFD using CVA-based control charts in the CSTR process.

when an IF occurs. By contrast, the others all tend to alarm sporadically, and thus behave more like false alarms. Overall, it can be seen that the developed method shows the best IFD performance among the static and dynamic MSPM methods being compared.

6. Conclusion and future perspective

In this paper, a weighted moving average (WMA) scheme has been combined with the Hotelling's T^2 statistic to form a WMA T^2 control chart (WMA-TCC). Compared with static MSPM methods such as PCA, WMA-TCC employs a time window and an optimal weight vector to improve its detection capability for IFs that always manifest themselves as repeated small and short fluctuations. Compared with traditional MA-based methods such as MA-PCA, WMA-TCC overcomes the problem of producing excessive false alarms when data exhibit autocorrelation, because it does not assume data to be independent. Moreover, WMA-TCC can use the correlation (autocorrelation and cross-correlation) information to increase its sensitivity to IFs by finding an optimal weight. Compared with dynamic MSPM methods such as DPCA and CVA, WMA-TCC selects the window length considering the characteristics of IFs, i.e., the fault duration and magnitude, and then gains additional sensitivity to IFs by optimizing its weight.

Existence of the optimal weight has been proven with the help of the Brouwer fixed-point theory and an iteration process to obtain the optimal weight has been provided. These ensure that the optimal WMA-TCC is implementable in real applications. Moreover, we

have found that the optimal weight possesses a symmetry structure, and an equal weight scheme is optimal when data exhibit no autocorrelation. This verifies the optimality of existing MA-based MSPM methods when applied to independent data. The proposed method has been evaluated using a numerical example and the CSTR process. Simulation results have shown that for IFs with same direction, magnitude and duration, the compared methods, including several well-known static and dynamic MSPM methods, fail to detect them whereas WMA-TCC succeeds in detecting them.

References

- [1] M. S. Choudhury, S. L. Shah, and N. F. Thornhill. Diagnosis of poor control-loop performance using higher-order statistics. *Automatica*, 40:1719–1728, 2004.
- [2] S. J. Qin. Statistical process monitoring: basics and beyond. *Journal of Chemometrics*, 17(8–9):480–502, 2003.
- [3] S. J. Wierda. Multivariate statistical process control—recent results and directions for future research. *Statistica Neerlandica*, 48(2):147–168, 1994.
- [4] A. Correcher, E. García, F. Morant, E. Quiles, and L. Rodríguez. Intermittent failure dynamics characterization. *IEEE Transactions on Reliability*, 61(3):649–658, 2012.
- [5] H. Y. Qi, S. Ganesan, and M. Pecht. No-fault-found and intermittent failures in electronic products. *Microelectronics Reliability*, 48(5):663–674, 2008.
- [6] B. Sun, S. K. Zeng, R. Kang, and M. Pecht. Benefits and challenges of system prognostics. *IEEE Transactions on Reliability*, 61(2):323–335, 2012.
- [7] L. K. Carvalho, M. V. Moreira, and J. C. Basilio. Diagnosability of intermittent sensor faults in discrete event systems. *Automatica*, 79:315–325, 2017.
- [8] J. F. Zhang, P. D. Christofides, X. He, F. Albalawi, Y. H. Zhao, and D. H. Zhou. Intermittent sensor fault detection for stochastic Itv systems with parameter uncertainty and limited resolution. *International Journal of Control*. Published online, DOI: 10.1080/00207179.2018.1490819.
- [9] S. Singh, H. S. Subramania, S. W. Holland, and J. T. Davis. Decision forest for root cause analysis of intermittent faults. *IEEE Transactions on Systems, Man, and Cybernetics, Part C: Applications and Reviews*, 42(6):1818–1827, 2012.
- [10] D. H. Zhou, Y. H. Zhao, Z. D. Wang, X. He, and M. Gao. Review on diagnosis techniques for intermittent faults in dynamic systems. *IEEE Transactions on Industrial Electronics*, Published online, DOI: 10.1109/TIE.2019.2907500, 2019.
- [11] O. Contant, S. Lafortune, and D. Teneketzis. Diagnosis of intermittent faults. *Discrete Event Dynamic Systems*, 14(2):171–202, 2004.
- [12] H. E. Garcia and T. S. Yoo. Model-based detection of routing events in discrete flow networks. *Automatica*, 41(4):583–594, 2005.
- [13] D. Lefebvre and E. Leclercq. Stochastic petri net identification for the fault detection and isolation of discrete event systems. *IEEE Transactions on Systems, Man, and Cybernetics-Part A: Systems and Humans*, 41(2):213–225, 2011.
- [14] S. Abdelwahed, G. Karsai, N. Mahadevan, and S. C. Ofsthun. Practical implementation of diagnosis systems using timed failure propagation graph models. *IEEE Transactions on Instrumentation and Measurement*, 58(2):240–247, 2009.

- [15] R. Y. Yan, X. He, and D. H. Zhou. Detection of intermittent faults for linear stochastic systems subject to time-varying parametric perturbations. *IET Control Theory & Applications*, 10(8):903–910, 2016.
- [16] R. Y. Yan, X. He, Z. D. Wang, and D. H. Zhou. Detection, isolation and diagnosability analysis of intermittent faults in stochastic systems. *International Journal of Control*, 91(2):480–494, 2018.
- [17] W. G. Zanardelli, E. G. Strangas, and S. Aviyente. Identification of intermittent electrical and mechanical faults in permanent-magnet ac drives based on time–frequency analysis. *IEEE Transactions on Industry Applications*, 43(4):971–980, 2007.
- [18] N. H. Obeid, A. Battiston, T. Boileau, and B. Nahid-Mobarakeh. Early intermittent interturn fault detection and localization for a permanent magnet synchronous motor of electrical vehicles using wavelet transform. *IEEE Transactions on Transportation Electrification*, 3(3):694–702, 2017.
- [19] J. Tian, C. Morillo, M. H. Azarian, and M. Pecht. Motor bearing fault detection using spectral kurtosis-based feature extraction and k-nearest neighbor distance analysis. *IEEE Transactions on Industrial Electronics*, 63(3):1793–1803, 2016.
- [20] B. P. Cai, Y. Liu, and M. Xie. A dynamic-bayesian-network-based fault diagnosis methodology considering transient and intermittent faults. *IEEE Transactions on Automation Science and Engineering*, 14(1):276–285, 2017.
- [21] H. Q. Ji, X. He, J. Shang, and D. H. Zhou. Incipient sensor fault diagnosis using moving window reconstruction-based contribution. *Industrial & Engineering Chemistry Research*, 55(10):2746–2759, 2016.
- [22] H. Q. Ji, X. He, J. Shang, and D. H. Zhou. Incipient fault detection with smoothing techniques in statistical process monitoring. *Control Engineering Practice*, 62:11–21, 2017.
- [23] J. Shang, M. Y. Chen, H. Q. Ji, and D. H. Zhou. Recursive transformed component statistical analysis for incipient fault detection. *Automatica*, 80:313–327, 2017.
- [24] S. Wold. Exponentially weighted moving principal components analysis and projections to latent structures. *Chemometrics and Intelligent Laboratory Systems*, 23(1):149–161, 1994.
- [25] J. H. Chen, C. M. Liao, F. R. J. Lin, and M. J. Lu. Principle component analysis based control charts with memory effect for process monitoring. *Industrial & Engineering Chemistry Research*, 40(6):1516–1527, 2001.
- [26] Wang Lin, Chun Jie Yang, and Youxian Sun. Multimode process monitoring approach based on moving window hidden markov model. *Industrial & Engineering Chemistry Research*, 57(1):292–301, 2018.
- [27] W. F. Ku, R. H. Storer, and C. Georgakis. Disturbance detection and isolation by dynamic principal component analysis. *Chemometrics and Intelligent Laboratory Systems*, 30(1):179–196, 1995.
- [28] U. Kruger, Y. Q. Zhou, and G. W. Irwin. Improved principal component monitoring of large-scale processes. *Journal of Process Control*, 14(8):879–888, 2004.
- [29] U. Kruger, S. Kumar, and T. Littler. Improved principal component monitoring using the local approach. *Automatica*, 43:1532–1542, 2007.
- [30] T. W. Anderson. *An Introduction to Multivariate Statistical Analysis (3rd edition)*. Wiley-Interscience, Hoboken, NJ, 2003.
- [31] S. J. Qin. Statistical process monitoring: basics and beyond. *Journal of Chemometrics*, 17(8-9):480–502, 2003.
- [32] C. F. Alcalá and S. J. Qin. Reconstruction-based contribution for process monitoring. *Automatica*, 45(7):1593–1600, 2009.
- [33] B. Mnassri, E. M. E. Adel, and M. Ouladsine. Generalization and analysis of sufficient conditions for pca-based fault detectability and isolability. *Annual Reviews in Control*, 37(1):154–162, 2013.
- [34] R. Isermann. Model-based fault-detection and diagnosis – status and applications. *Annual Reviews in control*, 29(1):71–85, 2005.
- [35] R. Dunia and S. J. Qin. A unified geometric approach to process and sensor fault identification and reconstruction: the unidimensional fault case. *Computers and Chemical Engineering*, 22(7–8):927–943, 1998.
- [36] R. Dunia and S. J. Qin. Subspace approach to multidimensional fault identification and reconstruction. *Aiche Journal*, 44(8):1813–1831, 1998.
- [37] S. J. Qin. Survey on data-driven industrial process monitoring and diagnosis. *Annual Reviews in Control*, 36(2):220–234, 2012.
- [38] S. Biswas. Diagnosability of discrete event systems for temporary failures. *Computers & Electrical Engineering*, 38(6):1534–1549, 2012.
- [39] D. G. Luenberger and Y. Ye. *Linear and nonlinear programming (3rd edition)*. Springer Science, New York, NY, 2008.
- [40] A. C. Chiang and K. Wainwright. *Fundamental methods of mathematical economics (4th edition)*. McGraw-Hill/Irwin, New York, NY, 2005.
- [41] E. Zeidler. *Nonlinear Functional Analysis and Its Applications I: Fixed-Point Theorems (1st edition)*. Springer-Verlag, New York, NY, 1986.
- [42] J. X. Sang, J. F. Zhang, T. X. Guo, D. H. Zhou, M. Y. Chen, and X. H. Tai. Detection of incipient faults in emu braking system based on data domain description and variable control limit. *Neurocomputing*, 383:348–358, 2020.
- [43] G. Li, S. J. Qin, Y. D. Ji, and D. H. Zhou. Reconstruction based fault prognosis for continuous processes. *Control Engineering Practice*, 18(10):1211–1219, 2010.
- [44] J. Shang, M. Y. Chen, H. Q. Ji, D. H. Zhou, and M. L. Li. Dominant trend based logistic regression for fault diagnosis in nonstationary processes. *Control Engineering Practice*, 66:156–168, 2017.
- [45] C. Shang, F. Yang, X. Q. Gao, X. L. Huang, J. A. K. Suykens, and D. X. Huang. Concurrent monitoring of operating condition deviations and process dynamics anomalies with slow feature analysis. *AIChE Journal*, 61(11):3666–3682, 2015.
- [46] K. E. S. Pilario and Y. Cao. Canonical variate dissimilarity analysis for process incipient fault detection. *IEEE Transactions on Industrial Informatics*, 14(12):5308–5315, 2018.